Chapter 4
A Mathematical Approach for Studying Ca^{2+}-Regulated Smooth Muscle Contraction

Saeil C. Murtada and Gerhard A. Holzapfel

Abstract Smooth muscle is found in various organs. It has mutual purposes such as providing mechanical stability and regulating organ size. To better understand the physiology and the function of smooth muscle different experimental setups and techniques are available. However, to interpret and analyze the experimental results basic models of smooth muscle are necessary. Advanced mathematical models of smooth muscle contraction further allow, to not, only investigate the experimental behavior but also to simulate and predict behaviors in complex boundary conditions that are not easy or even impossible to perform through *in vitro* experiments. In this chapter the characteristic behaviors of vascular smooth muscle, specially those relevant from a biomechanical point of view, and the mathematical models able to simulate and mimic those behaviors are reviewed and studied.

4.1 Introduction

Smooth muscle has an important role in hollow organs where it determines the size and the wall tension of the organ. In blood vessels the smooth muscle has a critical role in regulating the diameter and the flow resistance which affect the blood pressure.

To increase the understanding of both basic and clinical/pathophysiological processes of smooth muscle, well defined chemomechanical models which couple

S.C. Murtada (✉)
Division Genetic Physiology, Department of Physiology and Pharmacology, Karolinska Institutet, von Eulers väg 8, 177 71 Stockholm, Sweden
e-mail: saeil.murtada@ki.se

G.A. Holzapfel
Institute of Biomechanics, Center of Biomedical Engineering, Graz University of Technology, Kronesgasse 5-I, 8010 Graz, Austria
e-mail: holzapfel@tugraz.at

G.A. Holzapfel
Department of Solid Mechanics, School of Engineering Sciences, Royal Institute of Technology (KTH), Osquars Backe 1, 100 44 Stockholm, Sweden

chemical activation with mechanical contraction and relaxation are needed. The properties of the passive arterial wall have been thoroughly explored both in structural and mechanical behavior, and there are models available to capture these behaviors (Holzapfel et al., 2000; Holzapfel and Ogden, 2010; Schriefl et al., 2012). The properties of the active tone, which mainly originate from the active smooth muscle, have been less explored in both structure and contractile behavior, and there is a pressing need for well-defined models of the smooth muscle to better understand its mechanical properties.

In the following sections the characteristic smooth muscle behavior is described and followed up with some approaches of modeling smooth muscle contraction and active tension development. The main part of this chapter reviews and analyzes a certain mechanochemical modeling approach for smooth muscle (Murtada et al., 2010a, 2010b, 2012) which is based on structural observations and experimental data. It is the single model found in the literature which is able to simulate a realistic behavior of both smooth muscle active tension development at different stretches and a realistic muscle length behavior during isotonic quick-releases.

4.2 Smooth Muscle Behavior

Smooth muscle behaves differently in both activation and contraction and has a different underlying structure compared to skeletal and cardiac muscles. Therefore, it is important, when modeling and studying smooth muscle behavior, to understand and consider the characteristic behaviors and parameters relevant for smooth muscle contraction.

4.2.1 Myosin Kinetics

Smooth muscle contraction is regulated through phosphorylation and dephosphorylation of the myosin regulatory light-chains (MRLC) which is governed by two main enzyme activities, the myosin light-chain kinase (MLCK) and the myosin light-chain phosphatase (MLCP). By changing the membrane potential through depolarization, certain voltage-operated Ca^{2+} channels are opened, allowing an influx of Ca^{2+} which increases the cytoplasmic calcium. When the cytoplasmic intracellular calcium increases through an influx of Ca^{2+} from the extracellular matrix, the Ca^{2+} bind to the messenger protein calmodulin (CaM), which activates the MLCK. An alternative way to increase the cytoplasmic intracellular Ca^{2+} is through agonist stimulation, e.g., histamine which attaches to G protein coupled receptors (GPCR) that activate phospholipase C (PLC) which in turn induces inositol 1,4,5-triphosphate ($InsP_3$) production and Ca^{2+} release from the sarcoplasmic reticulum (SR) (Somlyo and Somlyo, 2002), see also Fig. 4.1.

When the myosin is phosphorylated, it can attach to the smooth muscle actin filaments through load-bearing cross-bridges that are able to perform power-strokes
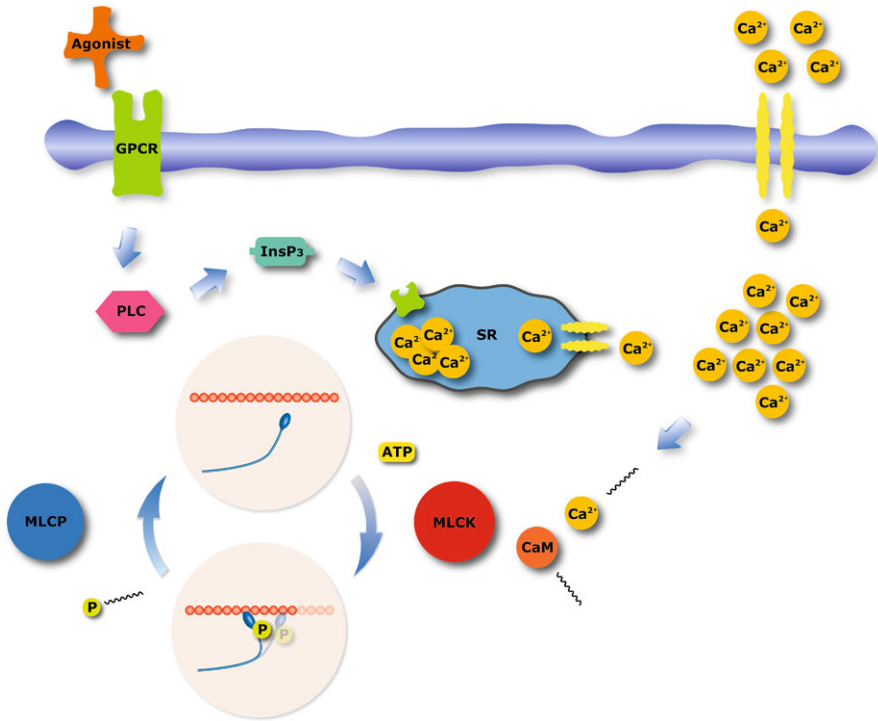
Fig. 4.1 Signaling pathways for Ca^{2+}-regulated myosin phosphorylation. Myosin phosphorylation/dephosphorylation is regulated by myosin light-chain kinase (MLCK) and myosin light-chain phosphatase (MLCP). MLCK is activated by a calmodulin (CaM)–Ca^{2+} complex which dependents on the level of intracellular $[Ca^{2+}]$. The intracellular Ca^{2+} may be influenced in different ways. Membrane depolarization and agonist stimulation through G protein coupled receptors (GPCR); during membrane depolarization certain channels on the cell membrane open resulting in an influx of Ca^{2+}. During agonist stimulation the GPCR activate phospholipase (PLC), which induces inositol 1,4,5-triphosphate (InsP3) production and releases Ca^{2+} from the sarcoplasmic reticulum (SR)

through ATP hydrolysis, similar as in skeletal muscle, causing muscle contraction. The MLCP activity, which governs the dephosphorylation of the myosin regulatory light-chains, has an effect on the Ca^{2+} sensitivity for the MRLC phosphorylation. There are several pathways inhibiting the MLCP, such as Rho-Rho kinase and protein kinase C. However, here we are not considering variations in MLCP activity. Smooth muscle is able to maintain active tension while the myosin phosphorylation decreases. An explanation for this phenomenon was hypothesized by introducing an attached, non-cycling (or slow-cycling), dephosphorylated cross-bridge (also known as latch-bridge or latched cross-bridge), see Dillon et al. (1981). The introduction of such as latched cross-bridge also explains the different contractile behaviors observed for isotonic quick-releases performed at different time after isometric activation (Dillon et al., 1981).
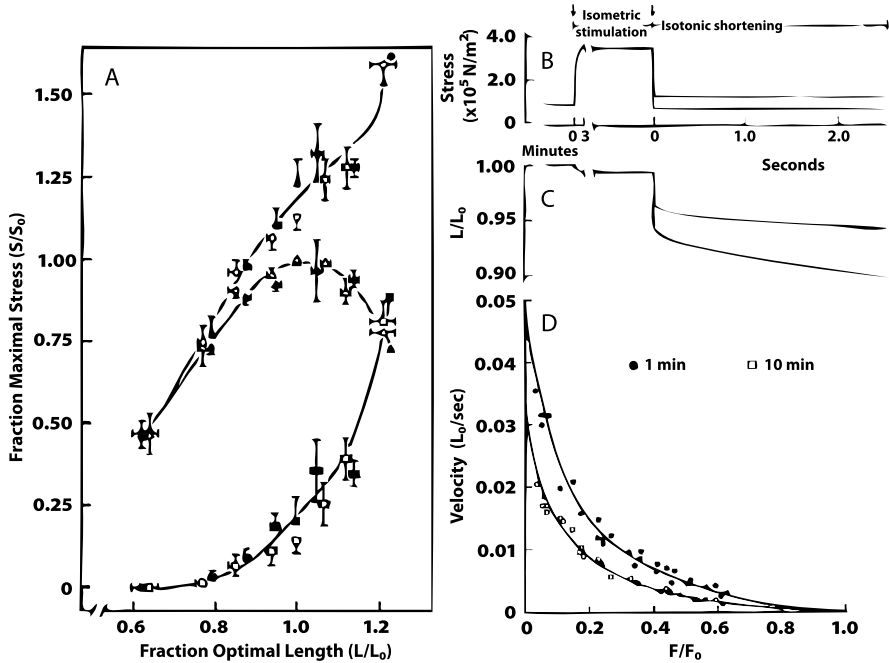
Fig. 4.2 **A**: length-tension behaviors of swine carotid media, where maximal steady-state active tension is obtained at a certain optimal length L_0. The *bottom curve* is the passive behavior, the *middle curve* is the active behavior and the *top curve* is the total behavior (passive and active) (Kamm et al., 1989). **B** and **C**: active stress development and stretch behavior during isometric stimulation and isotonic shortening for two different after-loads (Dillon et al., 1981). **D**: two force-velocity curves for isotonic quick-releases measured at 1 min and 10 min after isometric contraction at optimal length (Dillon et al., 1981)

4.2.2 Length-Tension Relationship

Smooth muscle is able to generate active tension over a broad range of muscle lengths. The active length-tension relationship has a parabolic behavior with maximal active tension at an optimal muscle length larger than the slack length, see Fig. 4.2A. In addition, Figs. 4.2B and C show the respective active stress development and stretch behavior during isometric stimulation and isotonic shortening for two different after-loads.

The origin of the active length-tension behavior, also found in skeletal muscle, is still not clearly distinguished but there are some hypothesis. One hypothesis is that the agonist sensitivity may be dependent on the stretch of the smooth muscle (Rembold and Murphy, 1990b). When the $[Ca^{2+}]$ was measured for the same concentration of agonist but at different muscle stretches, it was found that the magnitude of initial behavior of $[Ca^{2+}]$ function was different for different muscle stretches. Agonist stimulation (histamine, noradrenalin and so on) activates G protein-related pathways which leads to an increase in intracellular $[Ca^{2+}]$ to be different from

the direct membrane depolarizing stimulation (e.g., potassium) pathway, which also leads to an increase in intracellular [Ca^{2+}]. It should be noted that the length-tension relationship in smooth muscle is obtained for both membrane depolarization and agonist stimulation. A more plausible hypothesis is that the length-tension relationship may originate from the structural rearrangements within the smooth muscle contractile unit, when stretched. This would influence the filament overlap between the actin and myosin filaments in a smooth muscle contractile unit which has a direct relation to the number of attached cross-bridges, and hence the active tension produced by the smooth muscle. A connection between the length of the contractile unit (sarcomere) and the length-tension behavior in muscle has been hypothesized for a long time (Gordon et al., 1966).

4.2.3 Force-Velocity Relationship

The importance of the chemical and mechanical model combination is demonstrated when it comes to modeling the characteristic force-(shortening) velocity relationship of muscle. When the isotonic shortening velocity is measured for different forces (after-loads) a hyperbolic relationship of the force and the shortening velocity is obtained (Woledge et al., 1985). When extracting the force-velocity relationship, two certain times are of importance: (i) the time at which the quick-release is performed, i.e. the amount of time of isometric contraction before the quick-release, and (ii) the time at which the velocity is measured during the isotonic contraction.

   When the force-velocity relationship is extracted at different time of isotonic quick-release, the relationship changes. The shortening velocity is higher when the quick-release is performed at an early stage of the isometric contraction rather than at a later stage, see Fig. 4.2D. This behavior supports the hypothesis of non-cycling latch cross-bridges which are dominant at a later stage of an isometric contraction.

4.2.4 Smooth Muscle Modeling

By assuming the well-established three-element Hill muscle characteristic, as described by Fung (1970) for smooth muscle, the smooth muscle contractile unit is represented by an elastic serial element and a contractile element. The active tension produced by the smooth muscle depends on two main principal parameters: (i) the number of attached load-carrying cross-bridges, and (ii) the (average) elastic elongation of the attached cross-bridges, both phosphorylated and dephosphorylated (cf. Rachev and Hayashi, 1999; Yang et al., 2003; Stålhand et al., 2008; Murtada et al., 2010a).

   The kinetics of the smooth muscle myosin phosphorylation, which regulates the activation of smooth muscle contraction, can be used to define the number of attached load-carrying cross-bridges. The kinetics of myosin phosphorylation and

the number of load-bearing cross-bridges have been modeled through different approaches, see, e.g., Peterson (1982); Kato et al. (1984); Hai and Murphy (1988). In the myosin kinetics model by Hai and Murphy (1988) the latched cross-bridge was incorporated, and the myosin is described in four different functional states: (M) unattached and dephosphorylated, (Mp) unattached and phosphorylated, (AMp) attached and phosphorylated, (AM) attached and dephosphorylated. The two states where the myosin forms a cross-bride between the actin filament which can carry load are the attached states, AMp and AM. These functional states are coupled through different rate constants, where some can be related to the phosphorylating MLCK activity and some to dephosphorylating MLCP activity.

The average elastic elongation of the attached cross-bridges in the smooth muscle contractile unit is a key parameter to model the tension development in smooth muscle. It corresponds to the elastic serial element in the Hill muscle model. The average elastic elongation of the attached cross-bridges depends on the total deformation applied on the smooth muscle contractile unit and the sliding of actin and myosin filaments, which could be related to the contractile element in the Hill muscle model. It is necessary to model both the filament sliding and the average elastic elongation of the attached cross-bridges to simulate the length change and the tension development during muscle contraction. Among the smooth muscle models available in the literature there are some that also considers the filament sliding behavior to describe the active tension development and the total deformation of the smooth contractile unit (cf. Stålhand et al., 2008; Murtada et al., 2010a).

4.3 The Chemomechanical Response in Smooth Muscle—Results

In this section the modeling approach by Murtada et al. (2010a, 2010b, 2012) is briefly reviewed. This is an approach that is able to simulate both the length-tension and the force-velocity behavior of smooth muscle in addition to muscle contraction and relaxation regulated by $[Ca^{2+}]_i$.

In the work by Murtada et al. (2010a, 2010b, 2012), the model by Hai and Murphy (1988) was used to simulate the kinetics of the myosin functional states and the fraction of attached cross-bridges.

4.3.1 Cross-Bridge Kinetics Model

The active force produced by the smooth muscle is dependent on the number of attached cross-bridges in a smooth muscle contractile unit. The kinetics of attached cross-bridges is regulated by the MLCK and MLCP activity, which can be described by the cross-bridge kinetics model by Hai and Murphy (1988). Chemical kinetics
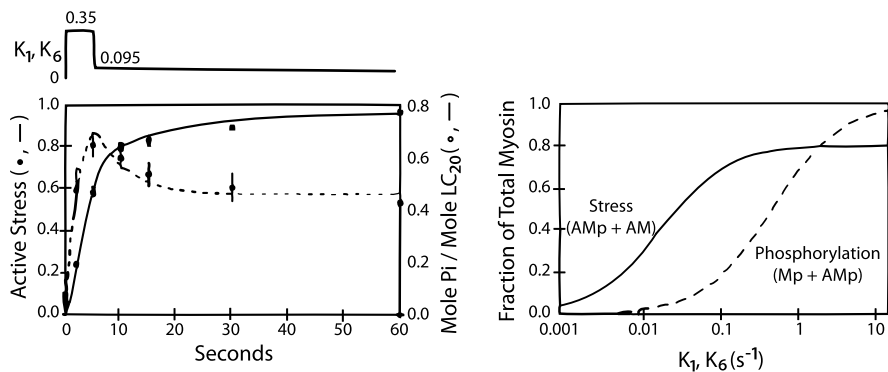
Fig. 4.3 *Left*: fitting results with the model by Hai and Murphy (1988) where the active stress is $n_{AMp} + n_{AM}$ and the myosin phosphorylation is $n_{Mp} + n_{AMp}$. The phosphorylating reaction rates k_1 and k_6 were set to 0.35 s^{-1} for 5 s followed by 0.085 s^{-1}. The other reaction rates were set to $k_2 = k_5 = 0.1$ s^{-1}, $k_4 = 0.11$ s^{-1}, $k_3 = 0.44$ s^{-1} and $k_7 = 0.005$ s^{-1}. *Right*: steady-state values of the sum of fractions $n_{AMp} + n_{AM}$ and $n_{Mp} + n_{AMp}$ for different values of the phosphorylating reaction rates k_1 and k_6 (Hai and Murphy, 1988)

can be summarized by the following system of differential equations, i.e.

$$\frac{d}{dt}\begin{bmatrix} n_M \\ n_{Mp} \\ n_{AMp} \\ n_{AM} \end{bmatrix} = \begin{bmatrix} -k_1 & k_2 & 0 & k_7 \\ k_1 & -(k_2+k_3) & k_4 & 0 \\ 0 & k_3 & -(k_4+k_5) & k_6 \\ 0 & 0 & k_5 & -(k_6+k_7) \end{bmatrix} \begin{bmatrix} n_M \\ n_{Mp} \\ n_{AMp} \\ n_{AM} \end{bmatrix},$$

(4.1)

where n_M, n_{Mp}, n_{AMp} and n_{AM} are fractions of the myosin functional states M, Mp, AMp, AM, with the constraint $n_M + n_{Mp} + n_{AMp} + n_{AM} = 1$, $n_i \geq 0$ and $k_1, \ldots, k_7$ are reaction rates describing the transition between the different functional states. Hence, the reaction rates k_1 and k_6 represents the phosphorylation of M to Mp and AM to AMp by the MLCK activity and the reaction rates k_2 and k_5 represents the dephosphorylation of Mp to M and AMp to AM by the MLCP activity. The reaction rates k_3 and k_4 represents the attachment and detachment of the cycling phosphorylated cross-bridges and the reaction rates k_7 represents the detachment of the latch-bridges. The phosphorylating reaction rates k_1 and k_6 can be coupled to the internal and also the external [Ca^{2+}]. Figure 4.3 shows the evolution of the different fraction of the functional states with time using the model by Hai and Murphy (1988).

When assuming maximal stimulated activation the phosphorylating MLCK activity can be related and coupled to the extracellular [Ca^{2+}]. In Murtada et al. (2010a) a Michaelis–Menten kinetics characteristic of the MLCK activity was implemented. The rate constants k_1 and k_6 are expressed as

$$k_1 = k_6 = \frac{[CaCaM]^2}{[CaCaM]^2 + K_{CaCaM}^2}, \qquad [CaCaM] = \alpha[Ca^{2+}]_e, \qquad (4.2)$$

where [CaCaM] is the concentration of the calcium-calmodulin complex, K_{CaCaM} is the half-activation constant, α is a positive constant and $[\text{Ca}^{2+}]_e$ is the external calcium concentration. In (4.2), $[\text{Ca}^{2+}]_e$ is not a function of time and the MLCK reaction rates are constant values.

The MLCK-activity can also be related to the intracellular $[\text{Ca}^{2+}]$ by using the first and fourth equations from (4.1) and setting $k_1 = k_6$ and $k_2 = k_5$. Thus (Murtada et al., 2010a),

$$k_1 = k_6 = \frac{k_2(n_{\text{Mp}} + n_{\text{AMp}}) - (\frac{\text{d}}{\text{d}t}n_{\text{M}} + \frac{\text{d}}{\text{d}t}n_{\text{AM}})}{n_{\text{M}} + n_{\text{AM}}}, \tag{4.3}$$

which in steady-state reduces to

$$k_1 = k_6 = \frac{k_2 \, \text{Phos}}{1 - \text{Phos}}, \tag{4.4}$$

where $\text{Phos} = (n_{\text{Mp}} + n_{\text{AMp}})$ is the fraction of phosphorylated cross-bridges (Rembold and Murphy, 1990a). The relationship between intracellular $[\text{Ca}^{2+}]$ and Phos was estimated in swine carotid SM by measuring aequorin light signal into a sigmoidal function, i.e.

$$\text{Phos} = -0.04 + \frac{0.686}{1 + 10^{-[3.645(0.004[\text{Ca}^{2+}]_i - 6.018) + 18.92]}}, \tag{4.5}$$

where $[\text{Ca}^{2+}]_i$ is the intracellular calcium concentration (Rembold and Murphy, 1990a). In a similar approach as for the external calcium concentration $[\text{Ca}^{2+}]_e$ in (4.2), the MLCK-activity can be related to the intracellular calcium concentration $[\text{Ca}^{2+}]_i$ according to

$$k_1 = k_6 = \varepsilon \frac{[\text{Ca}^{2+}]_i^h}{[\text{Ca}^{2+}]_i^h + (\text{ED}_{50})^h}, \tag{4.6}$$

where ε is a fitting parameter describing the maximal MLCK activity, h is a parameter related to the steepness of the relationship and ED_{50} is the half-activation constant for $[\text{Ca}^{2+}]_i$ to MLCK.

Through these approaches the external and intracellular calcium concentrations can be coupled to the fraction of the attached cross-bridges $n_{\text{AMp}} + n_{\text{AM}}$ by fitting the chemical parameters against dose-response relationships (Murtada et al., 2010a) or by comparing to myosin phosphorylation data (Murtada et al., 2010b, 2012).

4.3.2 Mechanical Model of the Smooth Muscle Contractile Unit

To introduce a description of the average elastic elongation of the attached cross-bridges in a smooth muscle contractile unit, and a related framework of the filament sliding evolution law to simulate filament sliding during contraction and relaxation, a mechanical model is necessary.

4.3.2.1 Mechanical Framework

In the recent works by Murtada et al. (2010a, 2010b, 2012) a description of a smooth muscle contractile unit based on structural observations (Herrera et al., 2005) and filament sliding theory was presented. The model of the smooth muscle contractile unit consists of two thin actin filaments, each with a certain length, and one thick myosin filament, with a certain length, which are overlapped. The actin filaments are organized on each side of the myosin filament from which the filament overlap L_o can be distinguished. Based on the Hill's muscle model, the length-change in a smooth muscle contractile unit is described by the relative actin and myosin filament sliding u_{fs} caused by the phosphorylated cycling cross-bridges or by an external load/deformation, and the elastic elongation u_e of the attached cross-bridges. Hence, the stretch of a contractile unit with reference length L_{CU} can be expressed as

$$\lambda = \frac{l_{CU}}{L_{CU}} = \frac{L_{CU} + u_{fs} + u_e}{L_{CU}}, \tag{4.7}$$

where l_{CU} is the deformed length of a contractile unit. Note that u_{fs} is denoted positive in extension. When looking at a half contractile unit, the average elastic elongation of the attached cross-bridges can be described by the average force acting on the contractile unit and the total elastic stiffness from all the attached cross-bridges. Thus,

$$\frac{u_e}{2} = \frac{\frac{P_a}{N_{CU}}}{(n_{AMp} + n_{AM})\frac{L_o}{\delta}E_{cb}}, \tag{4.8}$$

where P_a is the measurable active (averaged) first Piola-Kirchhoff stress (engineering stress), N_{CU} is the number of contractile units per unit area in the reference configuration, δ is the average distance between the cross-bridges, $(n_{AMp} + n_{AM})L_o/\delta$ is the total number of the attached cross-bridges and E_{cb} is the elastic stiffness of a single phosphorylated/dephosphorylated cross-bridge with the unit force per length. Together with Eq. (4.7) the active stress P_a can be derived as a function of the filament sliding u_{fs} and the stretch λ, i.e.

$$P_a = \mu_a \bar{L}_o (n_{AMp} + n_{AM})(\lambda - \bar{u}_{fs} - 1), \tag{4.9}$$

where $\mu_a = L_{CU}^2 E_{cb} N_{CU}/(2\delta)$ is a stiffness constant, $\bar{u}_{fs} = u_{fs}/L_{CU}$ is the normalized filament sliding and $\bar{L}_o = L_o/L_{CU}$ is the normalized filament overlap.

4.3.2.2 Evolution Law of Filament Sliding

The normalized filament sliding $\bar{u}_{fs}$ depends on the mechanical state (contraction and relaxation) of the smooth muscle contractile unit. During muscle contraction, $\bar{u}_{fs}$ is driven by the difference of the internal force of the cycling phosphorylated cross-bridges (AMp) and any external force acting on the contractile unit. During
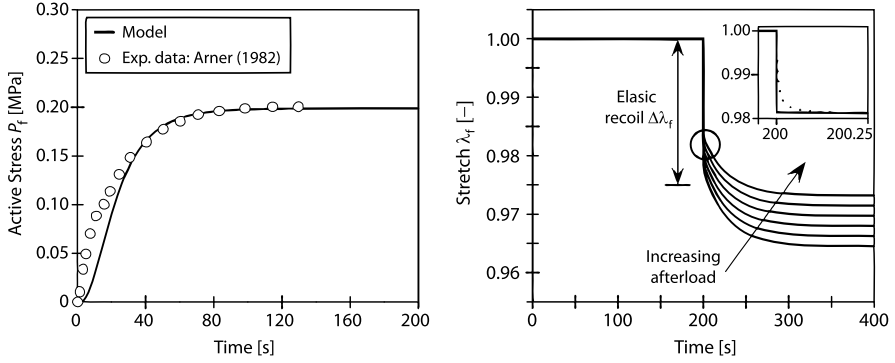
Fig. 4.4 *Left*: fitting results of the active stress development ($P_f = P_a$) using the model of Murtada et al. (2010a), with parameter values $\mu_a \bar{L}_o = 4.5$ MPa, $\eta = 60.0$ MPa s, $\kappa = 0.93$ MPa and $\mu_p = 0.90$ MPa. *Right*: isotonic stretch behavior ($\lambda_f = \lambda$) for different isotonic after-loads. The plot at the *top right corner* is an enlargement of the *encircled region* for a certain after-load (Murtada et al., 2010a). Compare with the experimental results presented in Figs. 4.2B and 4.2C

muscle relaxation (extension), $\bar{u}_{fs}$ is driven by the resulting force of the external force acting on the contractile unit, and the internal force from all the attached crossbridges (AMp, AM). The evolution law of $\bar{u}_{fs}$ is summarized as an active dashpot where the normalized filament sliding velocity $\dot{\bar{u}}_{fs}$ is proportional to the difference of the internal force P_c and the external active force P_a such as

$$\eta \dot{\bar{u}}_{fs} = P_c - P_a, \tag{4.10}$$

with

$$P_c = \begin{cases} \kappa n_{AMp}, & \text{for } P_a < \kappa n_{AMp}, \\ P_a, & \text{for } \kappa n_{AMp} \leq P_a \leq \kappa(n_{AMp} + n_{AM}), \\ \kappa(n_{AMp} + n_{AM}), & \text{for } P_a > \kappa(n_{AMp} + n_{AM}), \end{cases} \tag{4.11}$$

where η is a positive material parameter and κ is a parameter related to the average driving/resisting force of the attached cycling and non-cycling cross-bridges (AMp, AM).

The material parameters were fitted to isometric and isotonic contraction data performed on intact smooth muscle taenia coli (Arner, 1982), resulting to $\mu_a \bar{L}_o = 4.5$ MPa, $\eta = 60.0$ MPa s, $\kappa = 0.93$ MPa and $\mu_p = 0.90$ MPa (the parameter μ_p is the shear modulus of the passive matrix material of the smooth muscle cells and the intermixed fibrous components).

The model was able to predict the active tension development during isometric contraction and a realistic behavior of the muscle length change during isotonic contraction for different after-loads, see Fig. 4.4. However, with the current description of the $\bar{u}_{fs}$ evolution law and the constant filament overlap, the model is not able to predict the nonlinear behavior of the length-tension and the force-(shortening) velocity behavior.

4.3.3 Length-Tension and Force-Velocity Relationships

The ability for smooth muscle to produce active tension over a broad range of muscle lengths, with a maximal active tension development at an optimal muscle length, is an important characteristic to capture when simulating active smooth muscle contraction under large deformation. We have worked out the modeling of the length-tension behavior through two different approaches, briefly reviewed here. The model of Murtada et al. (2010a) served as a basis.

In the first approach, the effect of the intracellular calcium concentration $[Ca^{2+}]_i$ and the dispersion of contractile fibers in smooth muscles was investigated (Murtada et al., 2010b). In the second approach, the effect of filament overlap and filament sliding behavior in the smooth muscle contractile unit was analyzed (Murtada et al., 2012).

4.3.3.1 Agonist Sensitivity and Dispersion of Contractile Fibers

In the first approach of Murtada et al. (2010b), two experimental studies of smooth muscle were used to analyze stretch-dependent agonist sensitivity and the dispersion effects of contractile fibers in smooth muscles, see Fig. 4.5. This was then used as a basis for studying the smooth muscle length-tension behavior.

The intracellular calcium measurements at different muscle lengths was coupled with the Hai and Murphy reaction rates k_1 through Eqs. (4.4) and (4.5). The smooth muscle contractile units were modeled as in Murtada et al. (2010a) with an equivalent evolution law for the filament sliding $\bar{u}_{fs}$ and a constant filament overlap. The passive components in the surrounding matrix was modeled by elastin and one family of collagen fibers aligned along the main direction of the contractile units. The neo-Hookean material was used to model elastin and an anisotropic exponential function was used to model the anisotropic response (Holzapfel et al., 2000). The passive stress P_p of the surrounding matrix was derived as

$$P_p = \mu_p\left(\lambda - \frac{1}{\lambda^2}\right) + 2c_1\lambda\exp\left[c_2\left(\lambda^2 - 1\right)^2\right]\left(\lambda^2 - 1\right), \qquad (4.12)$$

where λ denotes the stretch in the loading direction and μ_p, c_1 and c_1 are material parameters. The passive material parameters (μ_p, c_1, c_2) were estimated by comparing the simulated stress-stretch behavior P_p through Eq. (4.12) with the passive length-tension experimental behavior of a carotid media (Kamm et al., 1989), with the results of $\mu_p = 1680$ Pa, $c_1 = 5040$ Pa and $c_2 = 0.20$ Pa.

The contractile unit orientation dispersion was modeled by introducing an orientation density function $\rho(\theta, \gamma)$ with rotational symmetry as a function of the angle θ and the parameter γ which describes the shape of the density function. Hence, the active stress P_a was expressed as

$$P_a = \mu_a\bar{L}_o(n_{AMp} + n_{AM})\frac{\lambda^\star + \bar{u}_{fs} - 1}{\lambda^\star}\left[\chi\left(\lambda - \frac{1}{\lambda^2}\right) + (1 - 3\chi)\lambda\right], \qquad (4.13)$$
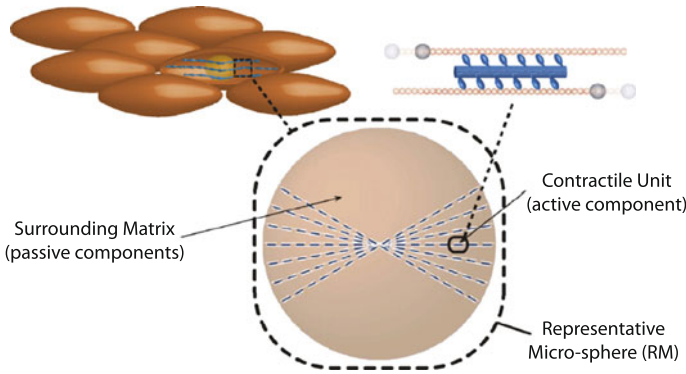
Fig. 4.5 According to Murtada et al. (2010b), smooth muscle cells are modeled through 'representative micro-spheres' which are divided into active and passive components. The active component is defined by the contractile units that are oriented in different directions and with a certain orientation density. The passive component is modeled by elastin and collagen fibers aligned in the main direction of the contractile units

where $\lambda^{\star} = [\lambda^2 + 2\chi(\lambda^{-1} - \lambda^2)]^{1/2}$, and $\chi \in [0, 1/3]$ is a dispersion parameter of the form

$$\chi = \pi \int_0^{\pi/2} \rho(\theta, \gamma) \sin^3\theta \, d\theta, \tag{4.14}$$

(cf. Gasser et al., 2006). For a detailed description of the choice and fitting of the orientation density function ρ see Murtada et al. (2010b).

The material parameters were estimated to fit the experimental data of active isometric tension development performed at two different muscle stretches, $\mu_a \bar{L}_o = 22.96$ MPa, $\eta = 2.215$ GPa s, $\kappa = 0.451$ MPa and $\chi = 0.016$. To study the effect of different orientation density functions ρ, the simulation was repeated for different values of γ, see Fig. 4.6.

When studying the length-tension behavior by modeling the stretch-dependent agonist sensitivity and the contractile unit orientation density function in smooth muscle, it was found that agonist sensitivity had a more significant effect on the length-tension behavior than the dispersion of the contractile units. The stretch-dependent agonist sensitivity could alone explain the length-tension behavior at the two studied muscle stretches. However, the $[Ca^{2+}]_i$ transient was only studied at two muscle stretches and it would be more convincing to study the agonist-sensitivity in smooth muscle with a more detailed set of experimental data of the $[Ca^{2+}]_i$ transient behavior for larger range muscle stretches. The length-tension behavior of smooth muscle exists for both agonist stimulations and membrane depolarization. However, studies show little significant change in the myosin phosphorylation behavior during potassium depolarization at different muscle lengths (Wingard et al., 1995), which contradicts a length-dependent sensitivity during membrane depolarization.
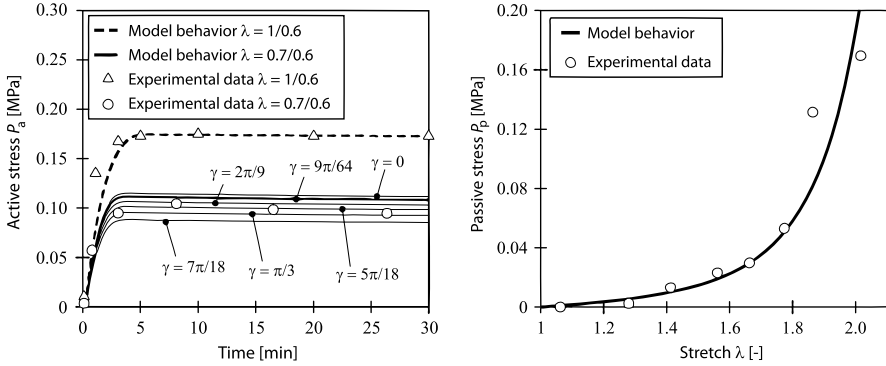
Fig. 4.6 *Left*: fitting results of the active stress developments at $\lambda = 1/0.6$ and $\lambda = 0.7/0.6$ by using the model of Murtada et al. (2010b). By repeating this for different orientation density functions $\rho(\gamma)$, where γ is a parameter describing the shape of the orientation density function, different behaviors of the predicted stress development at $\lambda = 0.7/0.6$ are obtained. *Right*: passive length-tension behavior (Murtada et al., 2010b). Compare with the passive length-tension behavior presented in Fig. 4.2A

4.3.3.2 Filament Overlap and Sliding Behavior

One common explanation for the length-tension behavior is the variation in the filament overlap in a contractile unit. This hypothesis was studied by introducing a filament overlap function $\bar{L}_o$ which defines the actin and myosin filament overlap and thereby the number of maximum possible attached cross-bridges in a contractile unit (Murtada et al., 2012). The filament overlap depends on the lengths of the actin and myosin filaments, and how these filaments slide with respect to each other, which was described by the normalized filament sliding $\bar{u}_{fs}$. An initial filament overlap $L_o(u_{fs} = 0) = x_0$ and an average optimal filament sliding u_{fs}^{opt}, for which optimal filament overlap is reached ($\partial L_o/\partial u_{fs}|_{u_{fs}=u_{fs}^{opt}} = 0$), were introduced. Thus the optimal filament overlap L_o^{opt} was defined as

$$L_o^{opt} = L_o\big(u_{fs} = u_{fs}^{opt}\big) = \frac{u_{fs}^{opt}}{2} + x_0. \tag{4.15}$$

Together with the boundary conditions, a continuous parabolic function of the filament overlap L_o was expressed as

$$L_o = u_{fs} - \frac{u_{fs}^2}{2u_{fs}^{opt}} + x_0 = \left(\bar{u}_{fs} - \frac{\bar{u}_{fs}^2}{2\bar{u}_{fs}^{opt}} + \bar{x}_0\right)L_{CU}, \tag{4.16}$$

where $\bar{x}_0 = x_0/L_{CU}$ and $\bar{u}_{fs}^{opt} = u_{fs}^{opt}/L_{CU}$, see Fig. 4.7.

The initial filament overlap $\bar{x}_0$ and the optimal filament overlap $\bar{u}_{fs}^{opt}$ were defined through two equations: the definition of the stretch of a contractile unit (4.7) at
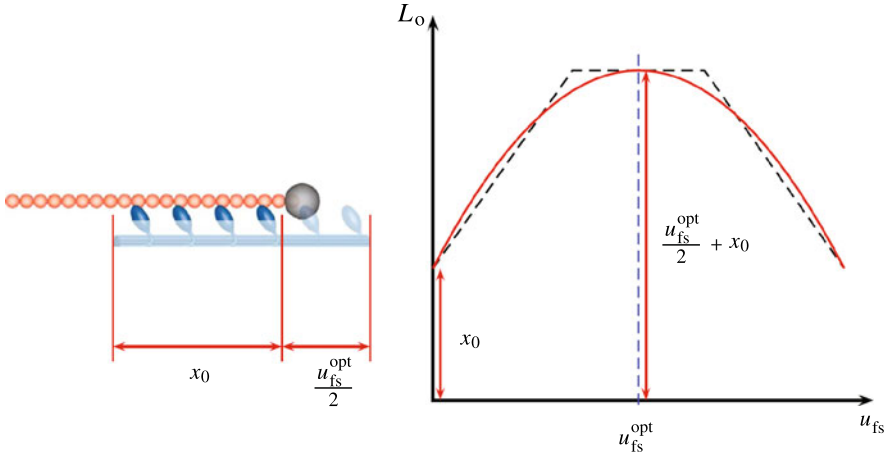
Fig. 4.7 Half contractile unit with the initial filament overlap x_0 between the myosin and actin filament. By introducing an optimal filament sliding distance u_{fs}^{opt} in a contractile unit, the filament overlap function L_o can be described by a parabolic function with an optimal filament overlap $u_{fs}^{opt}/2 + x_0$ (Murtada et al., 2012)

optimal muscle length, i.e.

$$\lambda_{opt} = 1 + \bar{u}_{fs}^{opt} + \bar{u}_e^{opt}, \tag{4.17}$$

where $\bar{u}_e^{opt} = u_e^{opt}/L_{CU}$, and by assuming that the fraction of the active stress at reference length P_0 and at the optimal length P_{opt} is equal to the fraction of the filament overlaps at the reference length and the optimal length, i.e.

$$\frac{P_0}{P_{opt}} = \frac{\bar{x}_0}{\bar{u}_{fs}^{opt}/2 + \bar{x}_0}. \tag{4.18}$$

Hence, the active stress of a contractile unit with varying filament overlap was expressed as

$$P_a = \mu_a \bar{L}_o(\bar{u}_{fs})(n_{AMp} + n_{AM})(\lambda - \bar{u}_{fs} - 1), \tag{4.19}$$

where $\bar{L}_o(\bar{u}_{fs}) = L_o(\bar{u}_{fs})/L_{CU}$.

One common way of studying the contractile mechanism in smooth muscle is to measure the shortening velocity during isotonic quick-release. The relationship between the shortening velocity and the after-load during isotonic quick-release can be described through a hyperbolic function, also known as Hill's equation (cf. Woledge et al., 1985), i.e.

$$(F + a)(v + b) = (F_0 + a)b, \tag{4.20}$$

where F is the isotonic after-load, F_0 is the isometric force at which the quick-release is performed, v is the muscle shortening velocity and a, b are fitting parameters. Based on the assumption that the velocity v reflects somewhat the behavior of

filament sliding $\bar{u}_{\text{fs}}$, which was supported by Guilford and Warshaw (1998), a similar hyperbolic function was used to redefine the evolution law of the relative filament sliding $\bar{u}_{\text{fs}}$, thus

$$(P_{\text{a}} + \alpha)(-\dot{\bar{u}}_{\text{fs}} + \beta) = (P_{\text{c}} + \alpha)\beta, \tag{4.21}$$

which can be rewritten as

$$\dot{\bar{u}}_{\text{fs}} = \beta \frac{P_{\text{a}} - P_{\text{c}}}{P_{\text{a}} + \alpha}. \tag{4.22}$$

When comparing the evolution law of the filament sliding $\bar{u}_{\text{fs}}$, as presented in Murtada et al. (2010a), with the updated evolution law (Murtada et al., 2012) it can be seen that the two evolution laws do not differ that much from each other.

The evolution law for $\bar{u}_{\text{fs}}$ was further extended to also allow the simulation of isotonic muscle extension such as

$$\dot{\bar{u}}_{\text{fs}} = \beta_1 \frac{P_{\text{a}} - P_{\text{c}}}{P_{\text{a}} + \alpha} - \beta_2 \frac{P_{\text{a}} - P_{\text{c}}}{P_{\text{a}} - P_{\text{LBC}}}, \tag{4.23}$$

where P_{LBC} is the maximal load-bearing capacity of the contractile units (yield stress) (Dillon et al., 1981), and β_1 and β_2 are fitting parameters. The internal stress P_{c}, which is governed by the number of attached cycling and non-cycling cross-bridges (depending on the mechanical state of the smooth muscle) is dependent on the varying filament overlap $\bar{L}_{\text{o}}$ as well. Hence, based on Eq. (4.11), the internal stress P_{c} during contraction was quantified as

$$P_{\text{c}} = \kappa_{\text{AMp}} \bar{L}_{\text{o}}(\bar{u}_{\text{fs}}) n_{\text{AMp}}, \tag{4.24}$$

and during muscle relaxation (extension) as

$$P_{\text{c}} = \kappa_{\text{AMp}} \bar{L}_{\text{o}}(\bar{u}_{\text{fs}}) n_{\text{AMp}} + \kappa_{\text{AM}} \bar{L}_{\text{o}}(\bar{u}_{\text{fs}}) n_{\text{AM}}, \tag{4.25}$$

where κ_{AMp} is a parameter related to the force due to a power-stroke of a single cross-bridge and κ_{AM} is related to the force-bearing capacity of a dephosphorylated attached (latch) cross-bridge during muscle extension.

The material parameters in the mechanical model were fitted to isometric tension development and to isotonic shortening velocities from swine carotid media (Dillon et al., 1981; Murtada et al., 2012), resulting in $\mu_{\text{a}} = 5.3$ MPa, $\alpha = 26.7$ kPa, $\beta = \beta_1 = 0.0083$ s^{-1} and $\kappa_{\text{AMp}} = 204$ kPa. The material parameters β_2 and κ_{AM} were fitted to sudden extension experiments resulting to $\beta_2 = 0.0021$ s^{-1} and $\kappa_{\text{AM}} = 61.1$ kPa. The parameters in the filament overlap function $\bar{L}_{\text{o}}$ were fitted to $\bar{u}_{\text{fs}}^{\text{opt}} = 0.48$ and $\bar{x}_0 = 0.8544$ by means of the conditions in Eqs. (4.17) and (4.18) together with length-tension experimental data from swine carotid media (Murtada et al., 2012). By using Eq. (4.19) together with a filament sliding evolution law and the kinetic model by Hai and Murphy (1988), the active stress P_{a} was simulated for different stretches λ, see Fig. 4.8. The simulated results show very good correlations with experimental data obtained from swine carotid media.
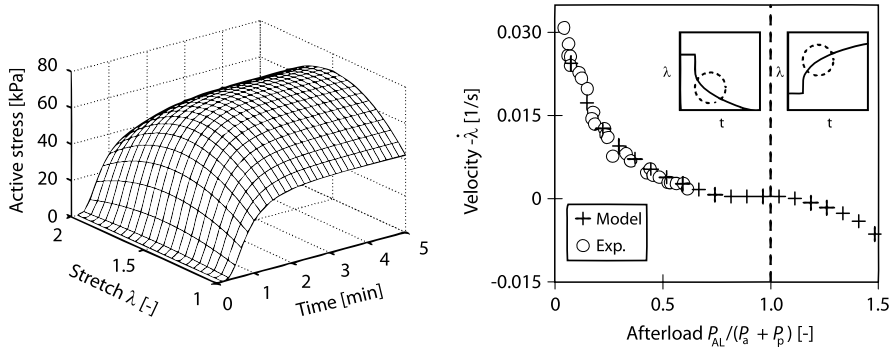
Fig. 4.8 *Left*: isometric active stress development for different muscle stretches λ activated by a certain intracellular calcium transient using the filament overlap model of Murtada et al. (2012); related material parameters are $\mu_a = 5.3$ MPa, $\alpha = 26.7$ kPa, $\beta = \beta_1 = 0.0083$ s^{-1} and $\kappa_{AMp} = 204$ kPa. *Right*: isotonic shortening and extension velocities for different after-loads (Murtada et al., 2012). Compare with the shortening velocity presented in Fig. 4.2D

Through the updated evolution law based on Hill's equation (4.22), the model was able to simulate a (very) realistic nonlinear behavior of the isotonic force-velocity relationship seen in smooth muscle. With the extended evolution law (4.23) a realistic behavior of the force development during sudden muscle extension and also the extension velocity were obtained. One of the advantages with the mathematical form of the extended filament sliding evolution law is the convenience of reducing it to its original form (4.22) when only simulating sudden muscle shortening.

4.4 Discussion and Concluding Remarks

In the present chapter, a review of a mathematical approach for studying smooth muscle contraction and relaxation was presented. There are several different smooth muscle models available in the literature and they have some characteristics in common, however the reviewed approach (Murtada et al. 2010a, 2010b, 2012) is one of the few which is able to simulate a realistic mechanochemical behavior of isometric contraction and relaxation at different muscle stretches and isotonic shortening/extension through one single model. The described approach models the active tension development by considering the number of attached cross-bridges, the average elastic elongation of attached cross-bridges and the filament sliding theory.

With the implemented filament overlap function, the model is able to simulate the well-known length-tension behavior which is very relevant for smooth muscle organs functioning at a large range of deformations. The model couples intracellular calcium [Ca^{2+}] with muscle contraction and relaxation through the Hai and Murphy myosin kinetics model (Hai and Murphy, 1988) and the smooth muscle model of Murtada et al. (2012). The myosin kinetics model describes the myosin

in four different functional states where two are load-bearings and coupled through seven reaction rates. The behavior of the active stress is proportional to the sum of the fractions of the load-bearing myosin functional states and is, therefore, very dependent on the behavior of the myosin kinetics model. However, it is not so trivial to define the reaction rates in the Hai and Murphy model and also to validate the simulated fraction values of attached cross-bridges. The Hai and Murphy kinetics model is rather old; it suggests the existence of a slower latch state myosin, where the myosin is dephosphorylated and attached, which has not been shown experimentally. In the last years several advances have been proposed in the understanding of myosin-actin kinetics so that an update of the myosin kinetics model would be a very valuable task.

The mechanical model presented in this chapter is based on structural observations and has a relatively low number of material parameters which can be related to the physical properties of the smooth muscle. For example, the physical parameter μ_a in the smooth muscle model (defined by the length of the contractile unit L_{CU}, the elastic stiffness of a single cross-bridge E_{cb}, the average distance between the cross-bridges δ and the contractile unit density N_{CU}) was investigated by comparing it with experimental data of L_{CU}, E_{cb}, δ and N_{CU}. It was found that it corresponds very well with the experimental data of the physical measurable units (Murtada et al., 2012) supporting the description and the fitted value of μ_a. However, there are still several items that can be improved such as an improved myosin kinetics model, which is not dependent on a latch state, and a further developed filament sliding evolution law.

With a realistic chemomechanical model of smooth muscle activity it is possible to study more complex boundary-value problems that are clinically and pathophysiologically relevant by implementing the coupled model into a three-dimensional finite element code. An implementation of the model into a finite element code also allows to study the effects of time-dependent changes in Ca^{2+} for different internal pressures of an intact artery that are relevant for both short-term and long-term changes in the vascular wall.

References

Arner A (1982) Mechanical characteristics of chemically skinned guinea-pig taenia coli. Eur J Physiol 395:277–284

Dillon PF, Aksoy MO, Driska SP, Murphy RA (1981) Myosin phosphorylation and the cross-bridge cycle in arterial smooth muscle. Science 211:495–497

Fung YC (1970) Mathematical representation of the mechanical properties of the heart muscle. J Biomech 269:441–515

Gasser TC, Ogden RW, Holzapfel GA (2006) Hyperelastic modelling of arterial layers with distributed collagen fibre orientations. J R Soc Interface 3:15–35

Gordon AM, Huxley AF, Julian FJ, (1966). The variation in isometric tension with sarcomere length in vertebrate muscle fibres. J Physiol 184:170–192

Guilford WH, Warshaw DM (1998) The molecular mechanics of smooth muscle myosin. Comp Biochem Physiol 119:451–458

Hai CM, Murphy RA (1988) Cross-bridge phosphorylation and regulation of latch state in smooth muscle. J Appl Physiol 254:C99–106

Herrera AM, McParland BE, Bienkowska A, Tait R, Paré PD, Seow CY (2005) Sarcomeres of smooth muscle: functional characteristics and ultrastructural evidence. J Cell Sci 118:2381–2392

Holzapfel GA, Gasser TC, Ogden RW (2000) A new constitutive framework for arterial wall mechanics and a comparative study of material models. J Elast 61:1–48

Holzapfel GA, Ogden RW (2010) Constitutive modelling of arteries. Proc R Soc A 466:1551–1597

Kamm KE, Gerthoffer WH, Murphy RA, Bohr DF (1989) Mechanical properties of carotid arteries from DOCA hypertensive swine. Hypertension 13:102–109

Kato S, Osa T, Ogasawara T (1984) Kinetic model for isometric contraction in smooth muscle on the basis of myosin phosphorylation hypothesis. Biophys J 46:35–44

Murtada S, Kroon M, Holzapfel GA (2010a) A calcium-driven mechanochemical model for prediction of force generation in smooth muscle. Biomech Model Mechanobiol 9:749–762

Murtada S, Kroon M, Holzapfel GA (2010b) Modeling the dispersion effects of contractile fibers in smooth muscles. J Mech Phys Solids 58:2065–2082

Murtada SC, Arner A, Holzapfel GA (2012) Experiments and mechanochemical modeling of smooth muscle contraction: significance of filament overlap. J Theor Biol 21:176–186

Peterson JW (1982) Simple model of smooth muscle myosin phosphorylation and dephosphorylation as rate-limiting mechanism. Biophys J 37:453–459

Rachev A, Hayashi K (1999) Theoretical study of the effects of vascular smooth muscle contraction on strain and stress distributions in arteries. Ann Biomed Eng 27:459–468

Rembold CM, Murphy RA (1990a) Latch-bridge model in smooth muscle: $[Ca^{2+}]_i$ can quantitatively predict stress. Am J Physiol 259:C251–C257

Rembold CM, Murphy RA (1990b) Muscle length, shortening, myoplasmic $[Ca^{2+}]$ and activation of arterial smooth muscle. Circ Res 66:1354–1361

Schriefl AJ, Zeindlinger G, Pierce DM, Regitnig P, Holzapfel GA (2012) Determination of the layer-specific distributed collagen fiber orientations in human thoracic and abdominal aortas and common iliac arteries. J R Soc Interface 9:1275–1286

Somlyo AP, Somlyo AV (2002) The sarcoplasmic reticulum: then and now. Novartis Found Symp 246:258–268

Stålhand J, Klarbring A, Holzapfel GA (2008) Smooth muscle contraction: mechanochemical formulation for homogeneous finite strains. Prog Biophys Mol Biol 96:465–481

Wingard CJ, Browne AK, Murphy RA (1995) Dependence of force on length at constant cross-bridge phosphorylation in the swine carotid media. J Physiol 488:729–739

Woledge RC, Curtin NA, Homsher E (1985) Energetic aspects of muscle contraction. Academic Press, San Diego

Yang J, Clark JW Jr, Bryan RM, Robertson C (2003) The myogenic response in isolated rat cerebrovascular arteries: smooth muscle cell model. Med Eng Phys 25:691–709